

---

EFDA–JET–CP(01)02-53

W.Fundamenski, G.Matthews, V.Riccardo, T.Eich, C.Ingesson, T.Kiviniemi,  
T.Kurki-Suonio, V.Philips, S.Sipilä and JET EFDA Contributors

# Power Exhaust in JET MkIIIGB ELMy H-modes



# Power Exhaust in JET MkIIIGB ELMy H-modes

W.Fundamenski, G.Matthews, V.Riccardo, T.Eich<sup>1</sup>, C.Ingesson<sup>3</sup>, T.Kiviniemi<sup>2</sup>,  
T.Kurki-Suonio<sup>2</sup>, V.Philips<sup>1</sup>, S.Sipilä<sup>2</sup> and JET EFDA Contributors\*

<sup>1</sup>*FZ Julich GmbH/Euratom, Institut für Plasmaphysik, TEC, D-52425 Julich, Germany*

<sup>2</sup>*Helsinki U. of Technology, Tekes-Euratom Assoc., PO Box 2200, FIN-02015 HUT, Finland*

<sup>3</sup>*FOM-Rijnhuizen, Ass. Euratom-FOM, TEC, PO Box 1207, 3430 BE Nieuwegein, NL*

*\*See appendix of the paper by J.Pamela "Overview of recent JET results",*

*Proceedings of the IAEA conference on Fusion Energy, Sorrento 2000*

Preprint of Paper to be submitted for publication in Proceedings of the  
EPS Conference,  
(Madeira, Portugal 18-22 June 2001)

“This document is intended for publication in the open literature. It is made available on the understanding that it may not be further circulated and extracts or references may not be published prior to publication of the original when applicable, or without the consent of the Publications Officer, EFDA, Culham Science Centre, Abingdon, Oxon, OX14 3DB, UK.”

“Enquiries about Copyright and reproduction should be addressed to the Publications Officer, EFDA, Culham Science Centre, Abingdon, Oxon, OX14 3DB, UK.”

## 1. MOTIVATION AND DESCRIPTION OF THE EXPERIMENT

The exhaust of power from a tokamak plasma is one of the key constraints on the design of a fusion reactor. The ITER divertor was designed on the basis of infra-red (IR) thermographic measurements of power deposition profiles in D-IIID, ASDEX-U and JT-60U, which indicate a broadening of the power profile with input power<sup>1,2</sup>. Recently a novel technique was developed at JET to measure time averaged power profiles using thermocouples (TC) embedded in the MkIIGB divertor plates. In its original form it involved the lifting of the strike point over a junction between vertical tiles on a shot-by-shot basis and inferring the power deposition profile as the spatial derivative of the partition of energy between the two tiles<sup>3</sup>. This method was very robust but too costly in shots for general application. For this reason an alternative method was developed involving the sweeping of the strike point over a thermocouple location within a single discharge and extracting the power profile using a finite element model of the tile<sup>4</sup>, Figs.1-2 (the two methods agree quite well at the outer target). Both methods indicate much narrower power profiles (higher peak wall loads) in high power ELMy H-modes, and the interpretation of this result is the main aim of the paper.

## 2. RESULTS AND ANALYSIS

Power deposition profiles were measured using the latter method in a series of 2.5MA/2.4T discharges involving a scan in the NBI heating power (4-18MW, where  $P_{L-H} \sim 5\text{MW}$ ) and a scan in  $D_2$  fuelling rate ( $0-3 \times 10^{22} \text{ s}^{-1}$ ). The outer peak heat flux is roughly five times larger than the inner one, Fig.3, so that the following discussion will focus on the outer target only. In L-mode, the heat flux decays exponentially away from the strike point, while in H-mode, a double exponential structure appeared on the outer target only, with a narrow e-folding length near the separatrix ( $\sim 3\text{mm}$  mapped to outer mid-plane) and a broader base profile elsewhere in the scrape-off-layer ( $\sim 5-7\text{mm-omp}$ ). Without gas puffing, the narrow layer was found to scale inversely with power entering the SOL,  $\lambda_{q, nw} \propto P_{\text{SOL}}^{-0.4 \pm 0.1}$ , while the base profile showed virtually no power dependence. At constant input power (12MW), the peak heat flux was strongly reduced by  $D_2$  puffing (from  $\sim 20$  to  $4\text{MW/m}^2$ ), with the narrow feature in the power profile effectively suppressed. Comparison of the total power profile (from TC analysis) with the electron power profile from Langmuir probes (LP), allowed the calculation of the ion power profile. Decomposition into the ion and electron channels, and into the double exponential (thin-wide) components, revealed a strong correspondence of the narrow layer with the ions, and of the base profile with the electrons, Figs.4-5 (here parallel heat flux is shown, where  $q_{\parallel}/q_{\text{target}} \sim 13$ ). The peak heat flux was dominated by the ions for  $P_{\text{SOL}} > 8\text{MW}$  (no gas puff) and for  $D_2$  puff rate  $< 10^{22} \text{ s}^{-1}$  (12MW).

Regression analysis of both scans led to the following scaling for the integral power width,  $\lambda_{q, \text{int}} \propto P_{\text{SOL}}^{-0.4 \pm 0.1} n_{\text{sep}}^{+0.4 \pm 0.1}$ , which is in sharp contrast to the ITER-99 scaling,  $\lambda_{q, \text{int}} \propto P_{\text{SOL}}^{+0.4 \pm 0.1}$ . Comparison of  $\lambda_{q, \text{int}}$  JET-TC with various theoretical models suggests neo-classical transport in the SOL, Fig.6 (for some effects, the pedestal density may be more relevant).

### 3. MODELLING AND INTERPRETATION

Modelling the SOL plasma using the OSM2/ERIENE coupled codes<sup>5,6</sup> lead to the following conclusions: a) Fluid modelling is insufficient to explain the observed asymmetry in the peak heat flux, b) in order to obtain global power balance, a ratio of ion to electron power entering the SOL of roughly 10 is required, c) although electrons remain collisional,  $v_e^* \sim 10-20$ , the ions become collisionless  $v_i^* \sim 1-2$  near the separatrix, d) the extracted radial heat diffusivities fall to neo-classical levels near the separatrix. Based on these results, ion orbit loss from the pedestal region was suggested as a candidate mechanism for explaining the narrow feature in the power deposition profile<sup>7</sup>. The ASCOT code<sup>8</sup> was used to investigate this effect using a three stage analysis: a) trace calculations on specified JET equilibria, b) self-consistent simulations with realistic pedestal profiles, c) grid based, coupled-code (ASCOT-OSM2/ EIRENE) simulations, with reconstructed 2-D SOL distribution of ions, electrons and neutrals. ASCOT is a 3-D Monte-Carlo guiding centre code, including all neo-classical effects (all drift terms) as well as ion-ion and ion-neutral collisions. Here we only present the final results. The inner and outer ion power deposition profiles obtained with ASCOT for the case without the SOL plasma and for various levels of the radial electric field in the SOL are shown in Fig.7a. Similar profiles with the SOL plasma from OSM2/EIRENE reconstruction are shown in Fig.7b. The effect of  $E_r$  is to increase the outer/inner asymmetry via the ExB drift, while SOL losses reduce the peak heat flux by  $\sim 50\%$ . The estimated  $E_r$  value for this shot was  $\sim 30-100$  kV/m, while the inner and outer peak ion heat flux estimates based on TC/LP analysis were  $9.4$  and  $4.5$  MW/m<sup>2</sup>. These values agrees with the ASCOT estimate for  $E_r \sim 55$  kV/m which is consistent with the field range cited above, although the profiles are even more narrow than observed experimentally. This could be due to interaction with the fluctuating E-fields which so far has not been included in the model.

### 4. COMPARISON OF LP, TC AND IR PROFILES

Infra-red thermographic<sup>9</sup> profiles of power deposition (obtained with the ABAQUS code) on the outer target differ visibly from both the TC & LP profiles, Fig.8. The difference is more pronounced in the H-mode case, where both the TC & LP profiles are much more narrow than in the L-mode, and skewed towards the SOL, while the TC profile remains roughly symmetric and of the same width as in the L-mode. The cause of this discrepancy is still unknown, but defocusing of the IR camera, either optical or digital, offers one possible explanation.

### 5. CONCLUSIONS AND CONSEQUENCES FOR ITER

The narrow feature in the power deposition profile, first observed in Ref.3 was confirmed by the new diagnostic technique, and modelling indicates that ion orbit losses are a probable cause of this effect. The profile width was found to decrease with input power and increase with separatrix density according to  $\lambda_{q, \text{int}} \propto P_{\text{SOL}}^{-0.4 \pm 0.1} n_{\text{sep}}^{+0.4 \pm 0.1}$ , in disagreement with the ITER-99 scaling. This new scaling predicts rather narrow power width in ITER (with neo-classical R and B

dependence,  $\lambda_{q, \text{int}} \sim 2.2 - 4.4\text{mm}$  vs.  $\sim 15\text{mm}$  with the ITER-99 scaling), but this is probably ameliorated by the higher neutral density in the ITER divertor suppressing direct orbit losses via charge exchange scattering; ASCOT simulations are planned to address this point. However, it is clear that due to lower upstream collisionality ( $v_{i, \text{sep}}^* \sim 0.5-1$ ), ion orbit losses will play an important role in ITER SOL and divertor physics.

## ACKNOWLEDGEMENTS

This work was conducted under European Fusion Development Agreement and was partly funded by EURATOM and the UK Department of Trade and Industry.

- [1]. ITER database, many authors, Nuclear Fusion, **39** (1999), 2423.
- [2]. A.Loarte, J. Nucl. Materials, **266-269** (1999), 99.
- [3]. G.F.Matthews et al., J. Nucl. Materials, **290-293** (2001), 668.
- [4]. V.Riccardo et al., Plasma Phys. Contr. Fusion, **43** (2001), 1.
- [5]. W.Fundamenski, Ph.D. Thesis, U.Toronto (1999).
- [6]. D.Reiter, J.Nucl. Materials, **196-198** (1992), 80.
- [7]. W.Fundamenski, J. Nucl. Materials, **290-293** (2001), 593.
- [8]. J.A.Heikkinen, Phys.Plasma, **4** (1997), 3655.
- [9]. T.Eich et al., “Analysis of Power deposition in JET MkIIIGB divertor by IR-thermography”, these proceedings.

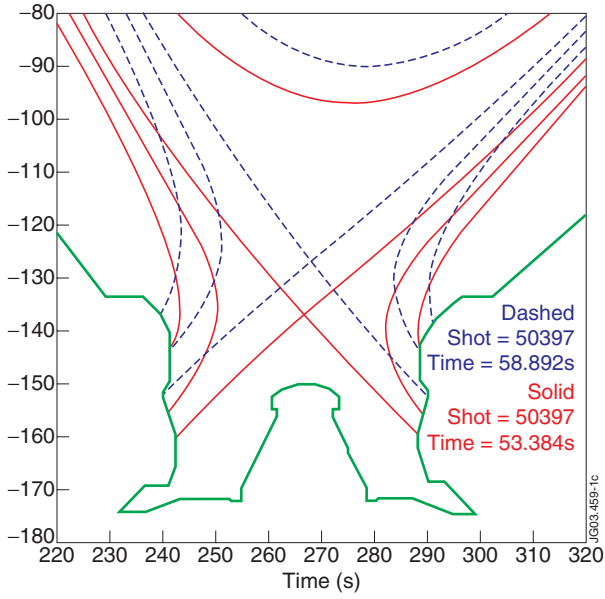


Figure 1: Initial and final positions of the vertical sweep used in the TC method.

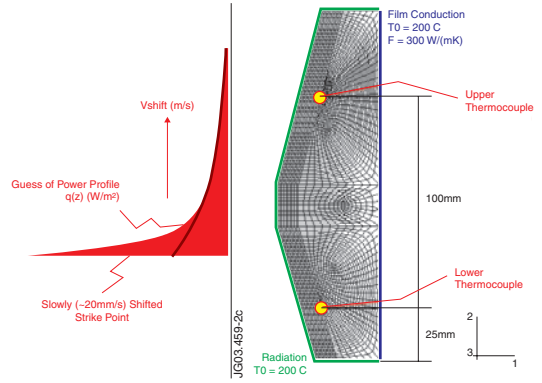


Figure 2: Finite Element model of the outer vertical tile and adjustable double exponential profile.

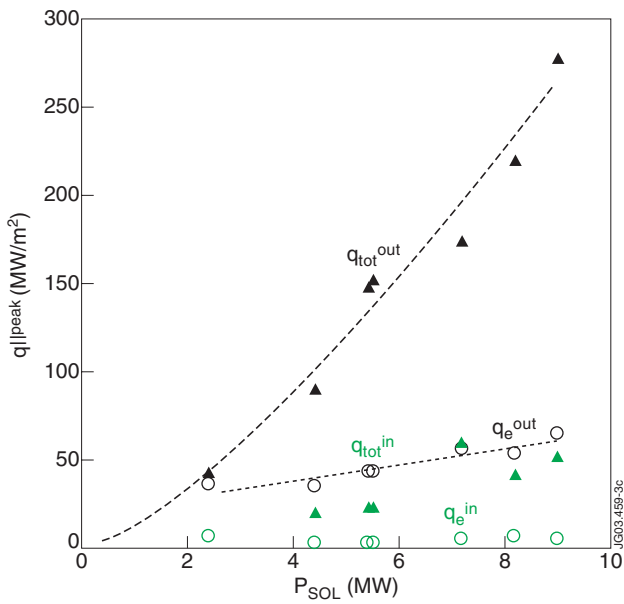


Figure 3: Total and electron peak heat flux values at the outer and inner targets; power scan.

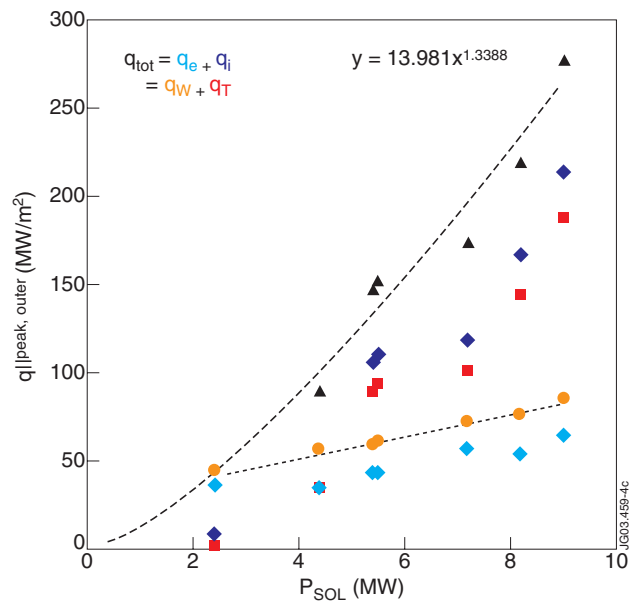


Figure 4: Outer peak heat flux in terms of the ion-electron and thin-wide components.



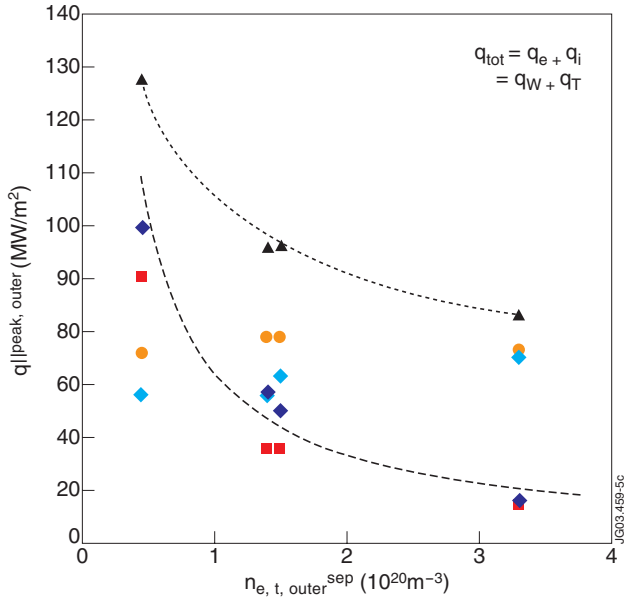


Figure 5: Similar to Fig.4, only for the gas puff (target density) scan.

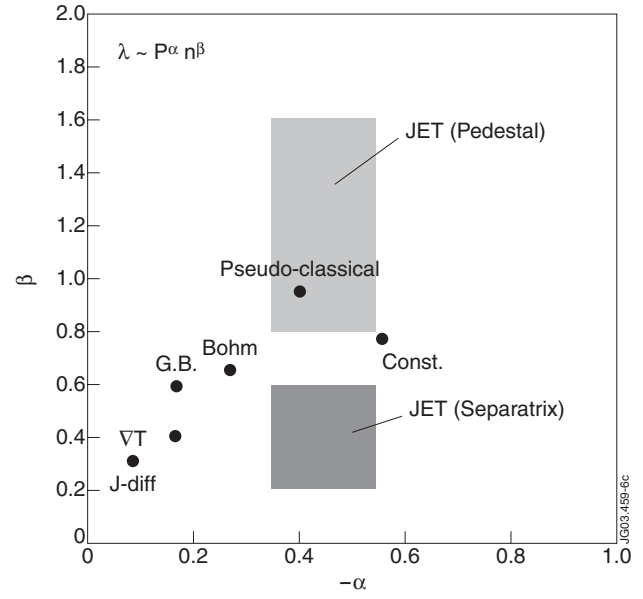


Figure 6: Comparison of various theories of SOL transport with the obtained scaling.

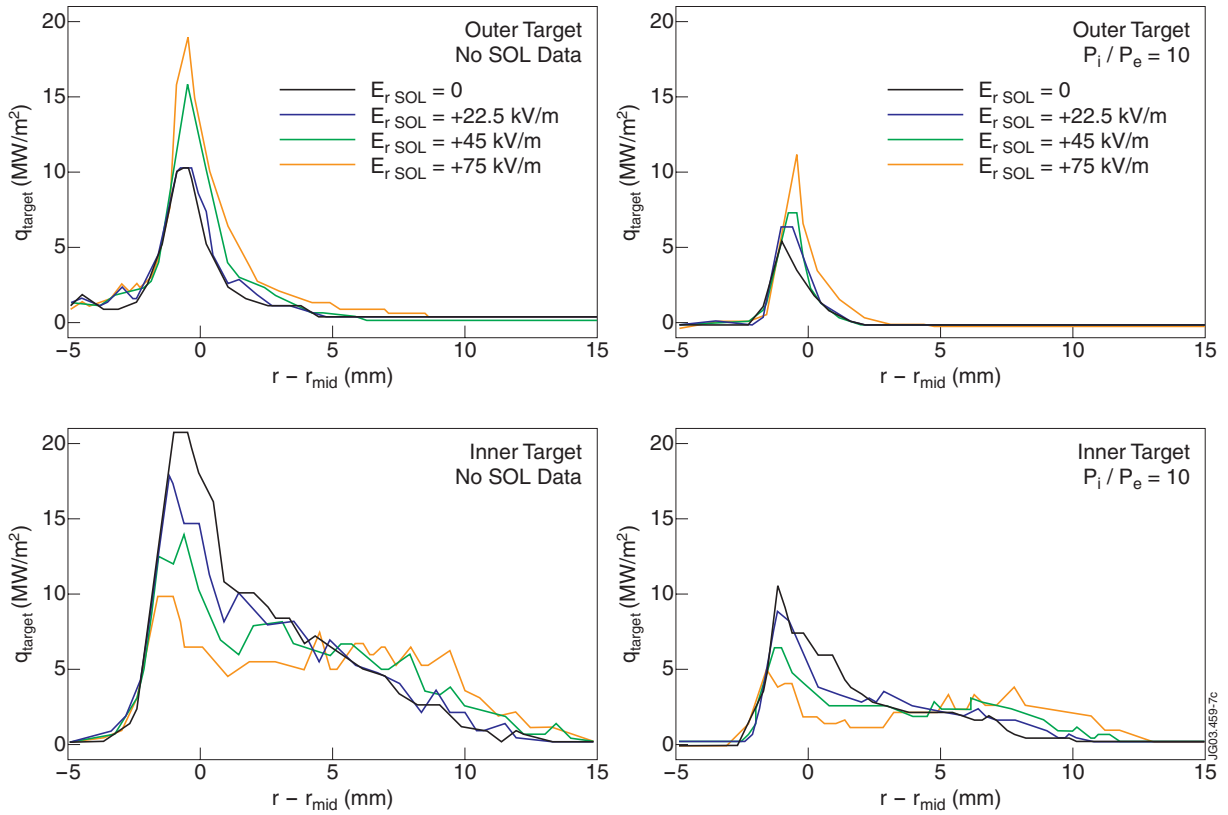


Figure 7: ASCOT target power profiles mapped to the outer mid-plane, for four levels of the radial electric field. On the left (a) is the no-SOL case, on the right (b) SOL with  $P_i/P_e = 10$ .

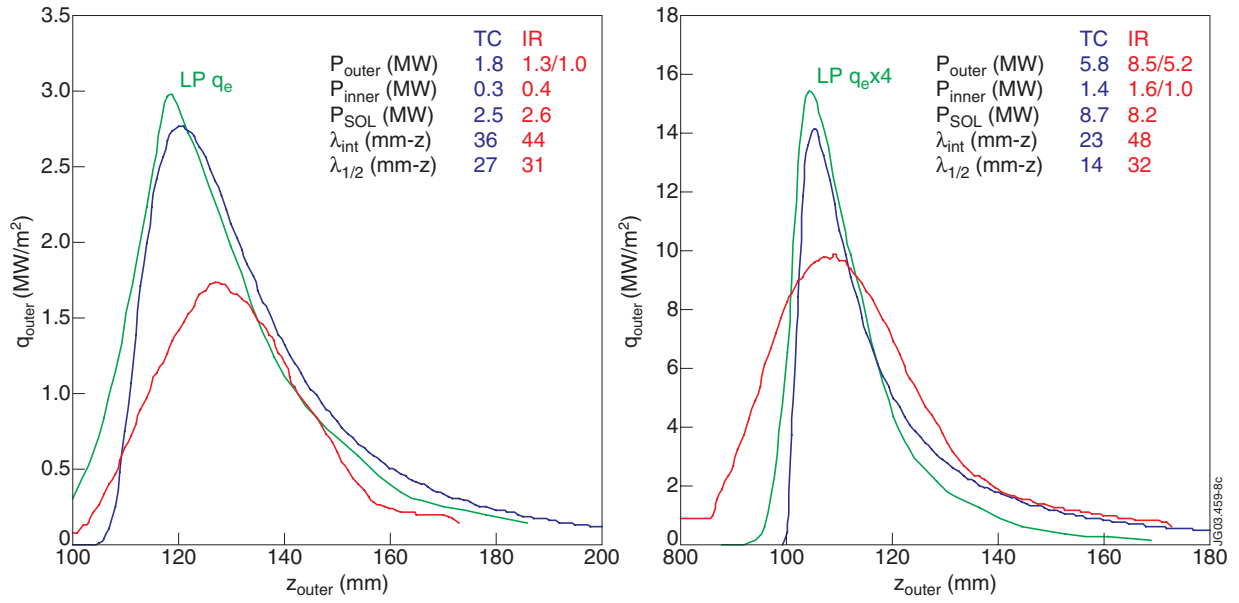


Figure 8: Comparison of Langmuir probe (LP), Thermocouple (TC) and Infra-Red (IR) profiles for 4MW L-mode (left) and 16MW H-mode (right).